Solar Cell Circuit Models: A Little Circuit Analysis

Tipale Kalpana Bhagwanrao, Department of Physics, Research Scholar, Ch.Charan Singh University, Meerut(U.P.)
Dr. Amit Juneja, Professor, Department of Physics, Ch.Charan Singh University, Meerut(U.P.)

Introduction

In order to interpret the data obtained from experimental measurements and to provide assistance in the process of optimizing a solar cell, it is absolutely necessary to have an equivalent circuit description of an organic solar cell. In the following few sections, the limitations of conventional solar cell circuit models will be discussed, and then various improvements will be shown.

Review Literature

P. K. Watkins and A. B. Walker 2015 A model system for blending polymers with electron-donating and -accepting chemicals has been created by our team. It has been discovered that the feature size should be around 10 nm in order to get the highest possible energy conversion efficiency. The first reaction method is used to describe the key processes in an organic solar cell using the dynamic Monte Carlo simulation. These processes include the generation, diffusion, and dissociation at the interface for excitons; the drift; the injection from the electrodes; and the collection by the electrodes for charge carries. According to the results of our calculations, it should be possible to achieve a power conversion efficiency (PCE) of 5% by achieving the optimal combination of charge mobility and shape. The characteristics that were employed in this model research correspond to a blend of new polymers known as bis(thienylenevinylene)-substituted polythiophene and poly(perylene diimide-alt-dithienothiophene), which possesses both a broad absorption and a high mobility. The I-V curves are accurately recreated by our simulations, and the power conversion efficiency (PCE) of the polymer mix can be as high as 2.2%. This is a higher value than the experimentally determined value (>1%), and it is one of the finest experimental findings currently known for all-polymer solar cells. Additionally, the dependence of PCE on charge mobility and the structure of the material is looked into as well.

K. Emery and M. A. Green, the year (2019)""Watkins et al. originally showed the utilization of a Dynamical Monte Carlo (DMC) model in order to predict charge transport in an organic solar cell . They modeled a polymer blend consisting of PFB and F8BT, and the results showed that the peak IQE for a bulk heterojunction was greater than 50%. This result is on the proper order when compared to the experimental observations. Watkins also proposed a way to construct bulk heterojunction morphologies with variable domain sizes. This approach was reported by Watkins. The section under "Model Description" will provide discussion on the specifics of this approach. In the study that Watkins did, determining the precise IQE of a device was not the primary goal; rather, it was verifying the validity of this kind of simulation and looking for broad trends. As a result, he made the following three important simplifications: There is no energy disorder for the localized hopping states, the exciton production rate was established by an order of magnitude calculation, and it was assumed to follow a Gaussian distribution with respect to the thickness of the solar cell. The mobility of holes and electrons is the same.

The C. W. Tang, (2011) Report. Fan Yang and Stephen Forrest utilized the DMC approach in order to replicate the prototypical small molecule organic system consisting of CuPc and C60 This was accomplished after Watkins provided evidence of the potential of the DMC method. In addition to this, they revised Watkins's too simplistic assumptions that they found to be incorrect. Both the equations and the Dynamic Monte Carlo approach may be used to analyze the novel material system. Yang and Forrest allowed for a difference in the mobility of holes and electrons, introduced a Gaussian energy disorder for the localized states, and calculated the exciton generation rate by multiplying the optical field intensity within the cell by the material absorption coefficient of the cell. This allowed for holes and electrons to have different levels of mobility. By increasing the precision of these aspects of

the model, Yang and Forrest were able to create simulated EQEs that were quite similar to those acquired through experimentation.

Conventional Solar Cell Equivalent Circuit Model-

Conventionally, a photo-voltaic device can be represented by the equivalent circuit model shown in fig. (a). Circuit model consists of a current source I_{ph} ' which models the photo-generated current, a diode D modeling the dark characteristic of the photo-voltaic cell, I is externally measured current and parasitic resistances R_s and R_{sh}, which are series resistance, representing the saturation of dark current and shunt resistance, representing the leakage current of diode respectively. Current source I_{ph} ' is connected in parallel to the diode.

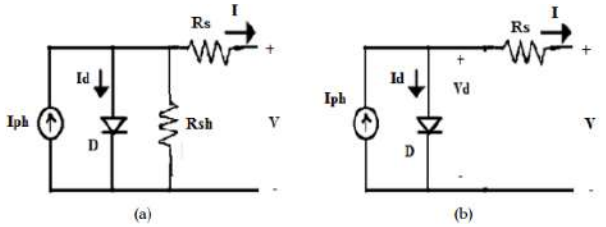

Fig.: Conventional equivalent circuit model of organic solar cell with series resistance R_s and shunt resistance R_{sh}.) Model of organic solar cell where effect of shunt resistance is absorbed in diode model.

If leakage currents are ignored or the effect of shunt resistance is absorbed in the diode D itself, equivalent model will simplify to that shown in fig. (b). For this model, externally measured current I can be modeled as

$$I = I_{ph} - f(V_D)$$

$$I = I_{ph} - f(V - IR_s)$$

Here, f(VD) represents the dark I-V characteristic of the device. In this model, photogenerated current I_{ph} is assumed to be only dependent on the incident light intensity and independent of the applied voltage V. this model has been used successfully for silicon photo-voltaic devices and attempts have been made to use this model for organic solar cells too, in the existing or modified form. But this model has some inherent problems. As an example, it predicts that open circuit voltage should increase with reduction in dark current.

$$I = I_{ph} - f(V_{OC} + 0) = 0$$

$$V_{OC} = f^{-1}(I_{ph})$$

Let us foe a moment assume that dark current can be modeled as exponentially dependent on the voltage like a p-n junction diode.

$$I_d = I_0\left(exp\left(\frac{V_d}{nV_{th}}\right) - 1\right)$$

Where, I_0 is reverse saturation current of diode, n is ideality factor and Vth is thermal voltage. Under open circuit condition I=0, from eq. $I_{ph} = I_d$ and $V_d = V_{OC}$. Eq. becomes-

$$I_{ph} = I_0\left(exp\left(\frac{V_{OC}}{nV_{th}}\right) - 1\right)$$

$$V_{OC} = nV_{th}\log\left(\frac{I_{ph}}{I_0} + 1\right)$$

Eq. predicts that open circuit voltage VOC of a photo-voltaic device can be increased by reducing reverse saturation current I_0 of the diode. In other words, one can say that by reducing the dark current of photo-voltaic cell, its open circuit voltage can be increased. Fig. shows two dark characteristics, one for carrier injection barriers of 0.3eV and another for 0.5eV. it can be seen that for barrier 0.5eV dark current is smaller than that of at 0.3eV barrier. In the same figure, photo-generated current for polaron pair generation rate

$G_x = 1 \times 10^{16} m^{-2} s^{-1}$ is also shown which is taken as

$I_{ph} = qG_x$

Where q denotes the charge of an electron. A standard model of a solar circuit would suggest that the open circuit voltage would be around 1.4 volts for a barrier height of 0.3 eV and around 1.5 volts for a barrier height of 0.5 eV. This would indicate that the open circuit voltage should grow as dark current decreases. However, it has been demonstrated in section that if leakage currents are neglected (which is the case here), the open circuit voltage of a photovoltaic device for varying barrier heights remains constant. This is in contrast to the predictions made by the standard model. The mismatch arises from the fact that it was assumed that the photo-generated current would be constant, which is not applicable for organic solar cells in general..

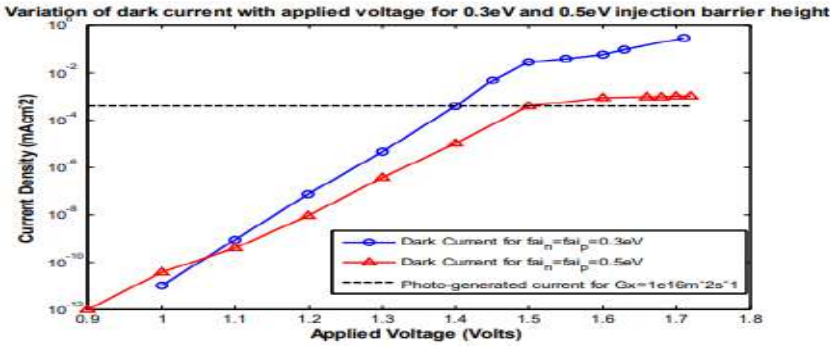

Fig.: Variation of dark current with applied voltage for 0.3eV and 0.5eV injection barrier heights G_x is polaron pair generation rate. $\mu_n = \mu_p = 1 \times 10^{-5} cm^2 V^{-1} s^{-1}$.

In more general model, the photo-generated current should be taken as a function of the voltage and eq. should be accordingly modified as

$I = I_{ph}(V - IR_s) - f(V - IR_s)$

To show this assertion, simulations were carried out for different injection barrier heights and mobility of $1 \times 10^{-5} cm^2 V^{-1} s^{-1}$ Current under dark and under light, for polaron pair generation rate of $1 \times 10^{20} m^{-2} s^{-1}$ are obtained. Difference of current under dark and current under light is taken as photo-generated current. Fig. shows the variation of photo-generated current I_{ph} with the voltage, for different injection barrier heights. Simulation results show a clear dependence of I_{ph} on the applied voltage. Fig. shows that as voltage increases, photo-generated current I_{ph} decreases and this change in photogenerated current with applied voltage is more pronounced for high barrier heights. For 0.6eV injection barrier height, I_{ph} changes by more than five orders of magnitude.

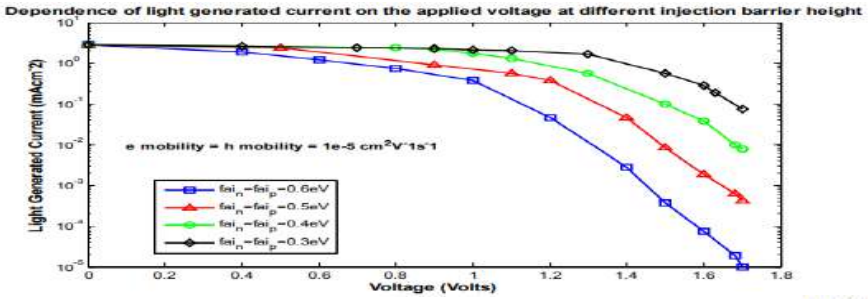

Fig.: Dependence of light generated current on the applied voltage. μ_n and μ_p are the electron and hole mobilities respectively. $\emptyset_n$ and $\emptyset_p$ are the injection barriers at cathode and anode respectively.

Fig. is re-plotted in fig. but this time taking photo-generated current to be voltage dependent. Fig. predicts open circuit voltage ~1.38 volts for 0.3eV injection barrier and ~1.4 volts for 0.5eV injection barrier. Open circuit voltage predicted at 0.5eV is quite same to that of predicted at 0.3eV from the fig., which was expected if leakage currents are ignored

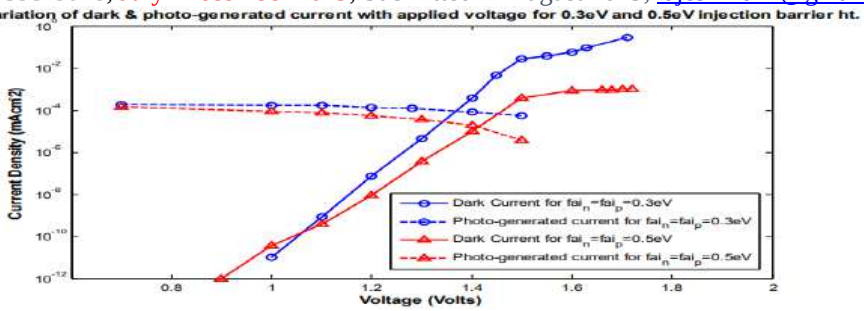

Fig.: variation of dark current with applied voltage for 0.3eV and 0.5eV injection barrier heights. Gx is polaron pair generation rate. Voltage dependent photo-generated current is also shown for two cases Fig.: variation of dark current with applied voltage for 0.3eV and 0.5eV injection barrier heights. Gx is polaron pair generation rate. Voltage dependent photo-generated current is also shown for two cases $\mu_n = \mu_p = 1 \times 10^{-5} cm^2 V^{-1} s^{-1}$.

Series Resistance in Organic Solar Cells-

It is well known that series resistance has a noteworthy negative impact on the characteristics of the solar cells. The series resistance is extracted from the dark characteristics and can be incorporated in equivalent circuit model in two distinct ways which leaves the dark characteristics unaltered.

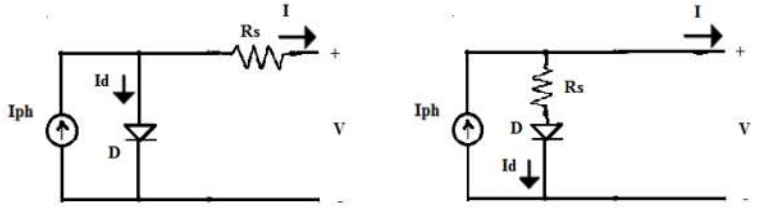

Fig.: solar cell equivalent model when (a) series resistance is placed in series of both current source I_{ph} and the diode D (b) series resistance is placed in series of diode D but in parallel of current source I_{ph}.

In fig.(a) series resistance has been placed in series with both current source I_{ph} and the diode D while in fig.(b) series resistance has been placed in series with diode D but in parallel to current source I_{ph}. In next section parameter extraction is done for the two models shown in fig. using the dark characteristics and subsequently, simulated light characteristics is fitted back using extracted parameters.

Extraction of Parameter and Fitting-

For the models presented in fig.(a) and (b), parameters are extracted from the simulated dark current and then light current is obtained from extracted parameters. To extract dark current parameters, photo-generated current I_{ph} is made zero. Note that if photo-generated current I_{ph} is made zero, both the circuit models shown in fig. (a) and (b) will reduce to same circuit that is diode D in series with series resistance Rs. so, extracted parameters from the dark characteristics will be same for both the models.

Diode current I_d is given by the equation

$$I_d = I_0 \left(exp\left(\frac{V_d}{n V_{th}}\right) - 1 \right)$$

Where n is ideality factor and V_{th} is thermal voltage. So, parameters to be extracted are reverse saturation current of diode I0, ideality factor n and series resistance R_s. To extract these parameters, current under dark and under light have been obtained for the injection barrier of 0.3eV and hole and electron mobility equal to $1 \times 10^{-5} cm^2 V^{-1} s^{-1}$ (fig.)

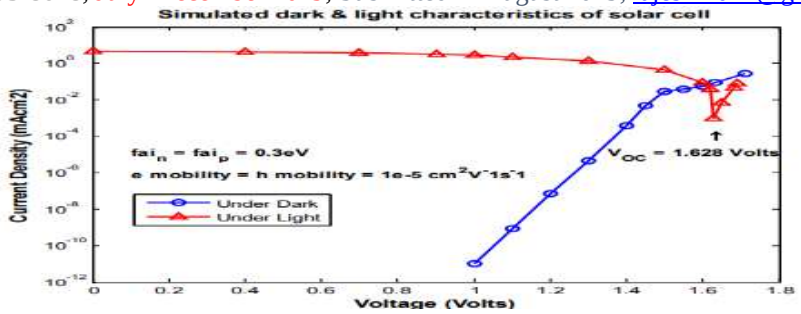

Fig.: Simulated dark and light characteristics of organic solar cell with both injection barrier heights of 0.3eV and electron and hole mobility

$\mu_n = \mu_p = 1 \times 10^{-5} cm^2 V^{-1} s^{-1}$ and $\Delta E_L = \Delta E_H = 0.5eV$.

In fig. initial part of the dark current is linear and can be fitted by only a diode. Later part, which shows saturation, is fitted with a diode and a resistance in series. Value of ideality factor n and reverse saturation current of the diode I_0 can be extracted by fitting the linear part. From the linear region of dark current in fig. we get

Ideality factor, n = 0.94

Reverse saturation current, $I_0 = 1.92 \times 10^{-29} mAcm^{-2}$

Series resistance, R_s = 0 ohm-cm ^{2}

Once the ideality factor n and reverse saturation currents I_0 are known, the saturated region of dark current can be fitted with a diode D, whose ideality factor n and reverse saturation currents I_0 are assumed to be same as estimated earlier and a series resistance which can be calculated in the following manner.

Applied voltage V is dropped across series resistance R_s and the diode D. if for applied voltage V, dark current is I_d.

$$V = I_d R_s + V_d$$

But,

$$V_d = nV_{th} \ln\left(\frac{I_d}{I_0}\right)$$

So

$$V = I_d R_s + nV_{th} \ln\left(\frac{I_d}{I_0}\right)$$

$$R_s = \frac{V - nV_{th} \ln\left(\frac{I_d}{I_0}\right)}{I_d}$$

Ideality factor n and reverse saturation currents I_0 having already been known, series resistance can be calculated from eq. Series resistance thus found will be voltage dependent. In fig. linear part of dark current ranges from 0 to 1.5 volts. Above 1.5 volts, dark current shows saturation and series resistance Rs comes out to be non-zero. Variation of series resistance Rs with applied voltage is shown in table

Table- Variation of series resistance, Rs with applied voltage for injection barrier of 0.3eV and $\mu_n = \mu_p = 1 \times 10^{-5} cm^2 V^{-1} s^{-1}$

Voltage (Volts)	0-1.5	1.6	1.628	1.7
R_s (Kohm cm^2)	0	1.414	1.0	0.66

Now, using extracted parameters light characteristic is obtained, using both the models shown in fig. (Model (a) and Model (b)) and plotted in fig. While calculating current under light, photo-generated current I_{ph} was treated as voltage dependent. Note that photo-

generated current was calculated by subtracting current under light from current under dark.

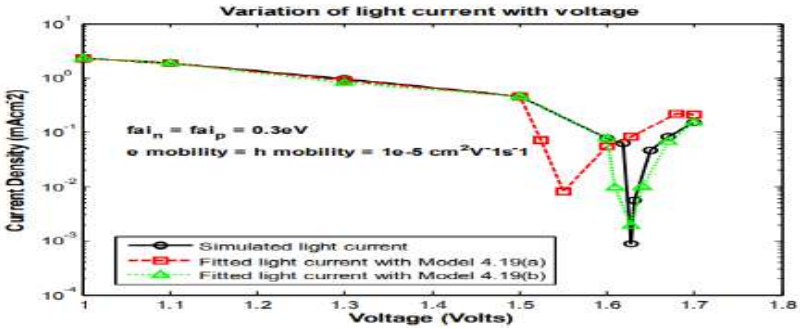

Fig.: Variation of light current is shown with voltage from simulated data (solid line), from fitting the model presented in (a) (dash) and from fitting the model presented in (b) (dotted line). Both injection barrier heights are 0.3eV and electron and hole mobility $\mu_n = \mu_p = 1 \times 10^{-5} cm^2 V^{-1} s^{-1}$ and $\Delta E_L = \Delta E_H = 0.5eV$.

From the fig. it is clear that solar cell circuit model shown in fig. (b) fits well for the extracted parameters, compared to the model shown in fig.(a). Solar cell circuit model shown in fig. (a) under estimates the open circuit voltage. It is important to notice that series resistance extracted above from the dark characteristic is internal resistance to the device. Now, suppose there is some external resistance also, say because of interconnect lines. For the moment assume that the interconnect offers 1.5 Kohm cm2 series resistance. I-V characteristic for 0.3eV injection barriers, carrier mobility of $\mu_n = \mu_p = 1 \times 10^{-5} cm^2 V^{-1} s^{-1}$ and with interconnect resistance of 1.5 Kohm cm2 is shown in fig.

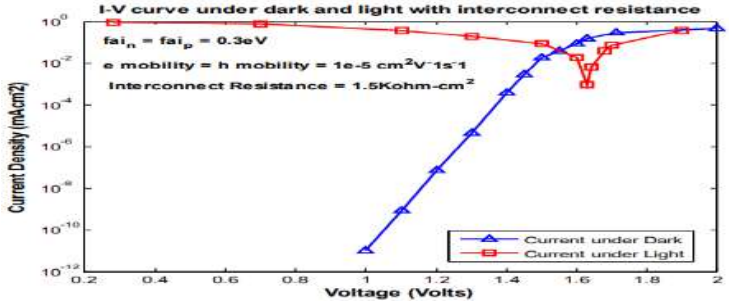

Fig.: Current under dark and light for injection barrier of 0.3eV, carrier mobility $\mu_n = \mu_p = 1 \times 10^{-5} cm^2 V^{-1} s^{-1}$ and ITO resistance of 1.5 Kohm-cm^2

We can extract ideality factor n, reverse saturation current I_0 and series resistance Rs, which will contain resistance from interconnect (R_{EXT}) and internal resistance of device (R_{INT}), from the dark characteristic shown in fig. Subsequently, we can fit the light characteristic shown in fig. from the extracted parameters. To fit light characteristic three models shown in fig. can be used. In model (a) total resistance (REXT+ RINT) is placed in series to diode D while in parallel to photo-current source I_{ph}. Model (b) places external resistance REXT, in series to both diode D and current source while internal resistance RINT comes in parallel to current source I_{ph} and series to diode D. model (c) incorporates total resistance in series to both the diode D and current source I_{ph}.

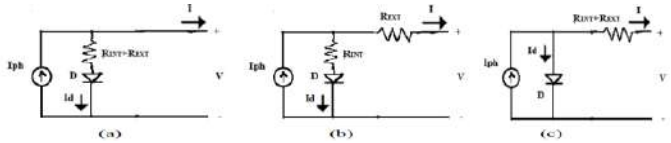

Fig.: Organic Solar Cell circuit model with (a) [Model (a)] total resistance $(R_{EXT}+ R_{INT})$ in parallel to current source (b) [Model (b)] R_{INT} in parallel and R_{EXT} in series to current source [Model (c)] total resistance $(R_{EXT}+ R_{INT})$ in series to current source.

The light characteristics of the models given in figure are suited to the simulated light characteristics, which are displayed in figure, It is evident from figure that the model of the solar cell circuit provided in figure (b) matches properly to the simulated data. On the other hand, the model presented in figure (a) overestimates the open circuit voltage, while the model shown in figure (c) under estimates the open circuit voltage. It is essential to take note that, when doing the extraction, we determined the overall resistance value to be $(R_{EXT}+ R_{INT})$. As a result of the fact that we were already familiar with the resistance value provided by the connecting lines, we were able to successfully match the simulated data using the model that is depicted in figure (b). It is often challenging to break the extracted series resistance when the internal resistance is combined with the exterior resistance. When the resistance of the environment is disproportionately high compared to the entire resistance, we can connect the total extracted resistance in series with the current source. I_{ph} both the data and the model that is depicted in figure (c) will line up quite well. On the other hand, if the internal resistance is the dominant factor, we can connect the total extracted resistance in parallel with the source of the current. I_{ph} and model represented in fig. (a) will be accurate enough to reproduce the characteristic of photo-voltaic device.

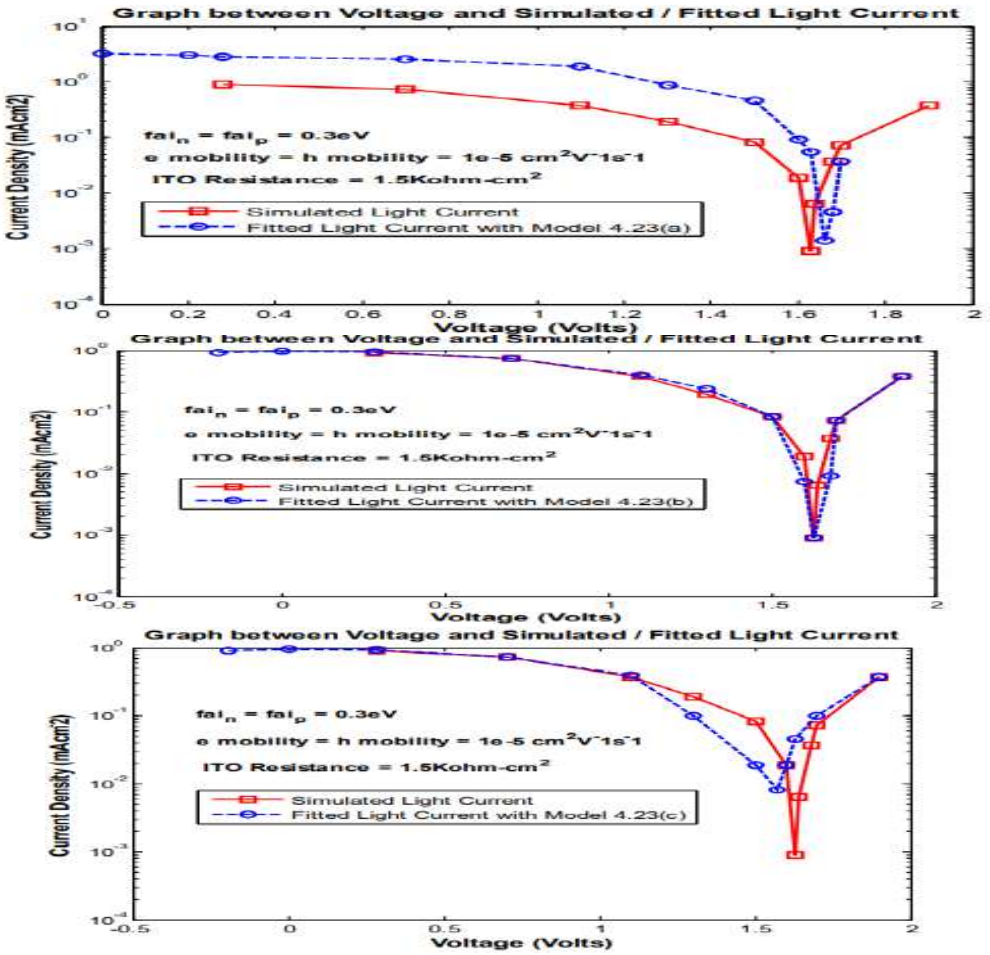

Fig.: Simulated (solid line) and fitted (dotted) light current, for model (a) shown in fig. (a), for the model (b) shown in fig.(b) and for model (c) shown in fig.(c). Injection barriers are 0.3eV, carrier mobility $\mu_n = \mu_p = 1 \times 10^{-5} cm^2 V^{-1} s^{-1}$ and ITO resistance of 1.5 Kohm-cm [2].

Constant Photo-Current Organic Solar Cell Model-

In each and every one of the parts that came before this one, photo-generated current I_{ph} during the process of data fitting and parameter extraction, it was assumed that the dependent variable was voltage. A model of a circuit for an organic solar cell is shown in this section. The model assumes that the photo-generated current is voltage independent. In

addition to that, the parameter extraction strategy for this model is explained. Figure depicts a model of an organic solar cell that assumes a photocurrent Ip that is unaffected by the voltage that is being applied and is instead just a function of the intensity of the incident light. In this model, the photocurrent Ip is proportional to the rate at which polaron pairs are generated. The shunt resistance is used to describe the loss that occurs as a result of polaron pair recombination at the hetero-junction interface. R_{sh} . and the series resistance Rs is used to simulate the process of charge extraction at the electrodes. Both series and shunt resistances are considered internal resistances to the device, as opposed to the exterior resistances that are typically associated with conventional models of solar cells. Only when light is present, due to the presence of perfect diodes D1 and D2, do the shunt and series resistances come into play. This model makes the assumption that the internal shunt resistance is constant. R_{sh} is independent of applied voltage while series resistance Rs is a function of applied voltage.

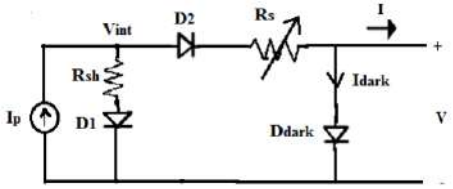

Fig.: equivalent circuit model of organic solar cell, which assumes photo-generated current I_p to be constant. Resistances R_{sh} and R_s models the recombination at heterojunction interface and extraction at electrodes respectively D_1 and D_2 are ideal diodes.

Parameter Extraction

- A method of extracting the series and shunt resistances is discussed in reference [12]. Here an alternative scheme is proposed to extract the model parameters.

From fig.

$$I_p = \frac{V_{int}}{R_{sh}} + I + I_{dark}$$

But, $V_{int} = V + (I + I_{dark})R_s$ so that

$$I_p = \left(\frac{R_s}{R_{sh}} + 1\right)(I + I_{dark}) + \frac{V}{R_{sh}}$$

R_{sh} is constant and if it is assumed that variation of R_s is small with voltage then differentiation of both sides of eq. gives

$$\left(\frac{R_s}{R_{sh}} + 1\right)\left(\frac{\partial I}{\partial V} + \frac{\partial I_{dark}}{\partial V}\right) + \frac{1}{R_{sh}} = 0$$

And,

$$I_p = qG_X$$

Parameter extraction is done for the simulated data shown in fig., where dark and light characteristics were obtained for injection barriers of 0.3eV and carrier mobilities $1 \times 10^{-5} cm^2 V^{-1} s^{-1}$ For the purpose of deriving the parameters, Equations and are concurrently solved with the applied voltage set to zero, and the values of the shunt and series resistances are determined. It is possible to compute the series resistance as a function of the voltage using the value of the shunt resistance and the equation. The calculated value of the shunt resistance was found to be 12.95 kilo-ohm-centimeter 2, and the values of the series resistance are displayed in figure as a function of voltage..

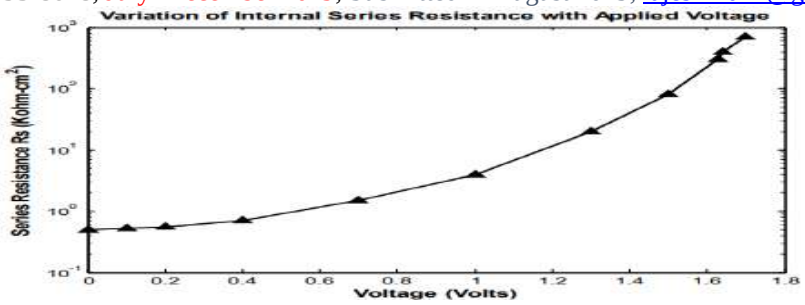

Fig.: Variation of internal series resistance with the applied voltage

It can be seen from the above figure that $\frac{\partial R_s}{\partial V} \cong 0$ at zero volts. For deriving eq. we assumed that variation of Rs is negligible with voltage and we used this equation at zero applied voltage only to extract the shunt and series resistance. The extracted values confirm that this assumption is really valid at zero applied voltage (see fig.).

Complete Organic Solar Cell Circuit Model-

Models of circuits for organic solar cells were covered in section of the chapter. These models assume that photo-current is voltage dependent. The circuit models for organic solar cells are given in figure, These models take into consideration the device's external and internal resistance. The location of these resistances in the circuit model was also considered; nevertheless, it was believed that photo-generated current was voltage dependant. A voltage independent photo-current was assumed to be flowing in section, and the resulting circuit model is depicted in figure. From these two parts, one may draw the conclusion that it is possible to conceive of a complete circuit model of an organic solar cell. This model would take into account internal and external resistances, as well as assume a voltage independent photocurrent. The schematic representation of this organic solar cell circuit may be found in figure.

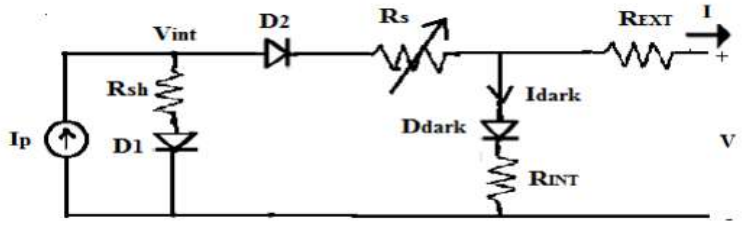

Fig.: Equivalent circuit model of organic solar cell, which assumes photo-generated current I_p to be constant and takes external and internal resistance into account. Resistances R_{sh} and R_s models the recombination at hetero-junction interface and extraction at electrodes respectively. D_1 and D_2 are ideal diodes. R_{INT} is the internal resistance to the device while R_{EXT} is external resistance.

Despite the fact that the model of an analogous organic solar cell circuit depicted in figure takes into consideration continuous photo-generated current, internal and exterior resistances, there are now additional parameters to extract. There is a single diode contained within this type. D_{dark} and three series resistances, R_s, R_{INT}, R_{EXT} to extract. Extraction of all these resistances individually poses a formidable challenge.

Conclusion:

It has been proved that if dark characteristics are supposed to follow an exponential current-voltage relationship, with an open circuit voltage and light produced current treated as constant, then an increase in the value of ideality factor will result in a reduction in the value of fill factor. This is the case even when an open circuit voltage and light generated current are taken as constant. If, on the other hand, dark features are supposed to follow a polynomial current-voltage relationship while the light produced current remains constant, then a rise in m will increase fill factor, which will become closer and closer to the value of 1. 6. In addition to the shape of the dark characteristic, it has been established that the

amplitude of the dark current measured at the open circuit voltage is an incredibly important component in estimating the fill factor of a device. This is the case even when the open circuit voltage is known. An increase in the dark current that is present when the open circuit voltage of a photovoltaic device occurs also leads in a rise in the fill factor of the photovoltaic device, as has been proved via the use of computer simulations. This relationship between the two variables has been established.

By utilizing the expression for the single diode exponential model, equations are built for the diode ideality factor n, reverse saturation current I0, series resistance Rs, shunt resistance Rsh, and photocurrent Iph. Following this step, the equations for the optimal load Rm, maximum power Pm, and fill factor FF are derived. Using the formulas for the double diode exponential model, equations for the saturation current I01 and I02 have been constructed. These equations may be found below. These equations pertain to the recombination and diffusion components of the space charge area, in addition to the shunt resistance Rsh and the photocurrent Iph. In the scenario of the double-diode exponential model, the value of Rs can be determined by employing either the quadratic solution method or the cubic solution method. When compared to the quadratic solution method, the accuracy of the parameter values that are represented by the cubic solution approach is significantly higher.

BIBLIOGRAPHY

[1] G. Feng, J. Li, Y. He, W. Zheng, J. Wang, C. Li, Z. Tang, A. Osvet, N. Li, C. J. Brabec, Thermal-driven phase separation of double-cable polymers enables efficient single-component organic solar cells, Joule 2019, 3, 1765.

[2] Y. Wu, J. Guo, W. Wang, Z. Chen, Z. Chen, R. Sun, Q. Wu, T. Wang, X. Hao, H. Zhu, A conjugated donor-acceptor block copolymer enables over 11% efficiency for single-component polymer solar cells, Joule 2019, 5, 1800.

[3] Z. Tang, W. Tress, Q. Bao, M. J. Jafari, J. Bergqvist, T. Ederth, M. R. Andersson, O. Inganäs, Improving cathodes with a polymer interlayer in reversed organic solar cells, Adv. Eng. Mater. 2014, 4, 1400643.

[4] J. Yao, B. Qiu, Z.-G. Zhang, L. Xue, R. Wang, C. Zhang, S. Chen, Q. Zhou, C. Sun, C. Yang, Cathode engineering with perylene-diimide interlayer enabling over 17% efficiency single-junction organic solar cells, Nat. Commun. 2011, 11, 1.

[5] C. Feng, X. Wang, Z. He, Y. Cao, Formation Mechanism of PFN Dipole Interlayer in Organic Solar Cells, Sol. RRL 2012, 5, 2000753.

[6] F. Zhang, A. Gadisa, O. Inganäs, M. Svensson, M. R. Andersson, Influence of buffer layers on the performance of polymer solar cells, Appl. Phys. Lett. 2004, 84, 3906.

[7] K. Sun, S. Zhang, P. Li, Y. Xia, X. Zhang, D. Du, F. H. Isikgor, J. Ouyang, Review on application of PEDOTs and PEDOT: PSS in energy conversion and storage devices, J. Mater. Sci.: Mater. Electron. 2015, 26, 4438.

[8] S. Jönsson, W. R. Salaneck, M. Fahlman, X-ray photoelectron spectroscopy study of the metal/polymer contacts involving aluminum and poly (3, 4-ethylenedioxythiophene)-poly (styrenesulfonic acid) derivatives, J. Mater. Res. 2003, 18, 1219.

[9] C. J. Brabec, S. E. Shaheen, C. Winder, N. S. Sariciftci, P. Denk, Effect of LiF/metal electrodes on the performance of plastic solar cells, Appl. Phys. Lett. 2012, 80, 1288.

[10] S. E. Shaheen, C. J. Brabec, N. S. Sariciftci, F. Padinger, T. Fromherz, J. C. Hummelen, 2.5% efficient organic plastic solar cells, Appl. Phys. Lett. 2001, 78, 841.

[11] R. Steim, S. A. Choulis, P. Schilinsky, C. J. Brabec, Interface modification for highly efficient organic photovoltaics, Appl. Phys. Lett. 2018, 92, 72.

[12] K. Lee, J. Y. Kim, S. H. Park, S. H. Kim, S. Cho, A. J. Heeger, Air- stable polymer electronic devices, Adv. Mater. 2017, 19, 2445.

[13] S. Bai, Y. Jin, X. Liang, Z. Ye, Z. Wu, B. Sun, Z. Ma, Z. Tang, J. Wang,U. Würfel,

Ethanedithiol treatment of solution-processed ZnO thin films: controlling the intragap states of electron transporting interlayers for efficient and stable inverted organic photovoltaics, Adv. Eng. Mater. 2015, 5, 1401606.

[14] Y. Sun, J. H. Seo, C. J. Takacs, J. Seifter, A. J. Heeger, Inverted polymer solar cells integrated with a low-temperature-annealed sol-gel- derived ZnO film as an electron transport layer, Adv. Mater. 2011, 23, 1679.

[15] J. Bertrandie, J. Han, C. S. De Castro, E. Yengel, J. Gorenflot, T. Anthopoulos, F. Laquai, A. Sharma, D. Baran, The energy level conundrum of organic semiconductors in solar cells, Adv. Mater. 2015, 34, 2202575.

[16] X. e. Li, Q. Zhang, J. Yu, Y. Xu, R. Zhang, C. Wang, H. Zhang, S. Fabiano, X. Liu, J. Hou, Mapping the energy level alignment at donor/acceptor interfaces in non-fullerene organic solar cells, Nat. Commun. 2019, 13, 1.

[17] S. Xiong, L. Hu, L. Hu, L. Sun, F. Qin, X. Liu, M. Fahlman, Y. Zhou, 12.5% flexible nonfullerene solar cells by passivating the chemical interaction between the active layer and polymer interfacial layer, Adv. Mater. 2019, 31, 1806616.

[18] X. Zhu, L. Hu, W. Wang, X. Jiang, L. Hu, Y. Zhou, Reversible chemical reactivity of non-fullerene acceptors for organic solar cells under acidic and basic environment, ACS Appl. Energy Mater. 2019, 2, 7602.

[19] Q. Kang, Q. Wang, C. An, C. He, B. Xu, J. Hou, Significant influence of doping effect on photovoltaic performance of efficient fullerene-free polymer solar cells, J. Energy Chem. 2017, 43, 40.